Draft version July 8, 2021
Typeset using LaTeX **preprint** style in AASTeX63

The DESI PRObabilistic Value-Added Bright Galaxy Survey (PROVA-BGS) Mock Challenge

ChangHoon Hahn,[1,2,*] Gyubin Kwon, Malgorzata Siudek, Rita Tojeiro, and GQP WG

[1] *Lawrence Berkeley National Laboratory, 1 Cyclotron Rd, Berkeley CA 94720, USA*
[2] *Berkeley Center for Cosmological Physics, University of California, Berkeley CA 94720, USA*

ABSTRACT

In this project, we present the methodology for inferring physical properties of galaxies from joint SED fitting of the DESI optical photometry and spectroscopy. We construct realistic forward modeled DESI data from star formation and chemical enrichment histories of galaxies in the L-Galaxies semi-analytic model and the Illustris TNG hydrodynamic simulations. Then, using these mock observations, we demonstrate that the stellar mass and SFR posteriors from our SED fitting are consistent with constraints from other SED fitting methods in the literature and, more importantly, the input stellar masses and SFRs from the simulations. The SED fitting we present and validate in this project will be used to construct the PRObabilistic Value-Added Bright Galaxy Survey (PROVABGS) from DESI observations.

Keywords: keyword1 – keyword2 – keyword3

1. INTRODUCTION

The Dark Energy Spectroscopic Instrument will conduct the largest spectroscopic galaxy survey to date covering $\sim$14,000 deg^2 (**?**). Over the next five years,

TODO What is DESI? Provide an overview of DESI specifics, numbers, and science goals, which will mostly be cosmology (BAO, RSD, etc). DESI will be great Beyond its impact on cosmology, DESI will also be transformative for galaxy science.

provide value-added galaxy catalogs (VAGCs), which will be transformative for galaxy science. In the past, VAGCs such as the MPA-JHU[1] provided galaxy properties from emission line analyses of SDSS spectra **?**.

Similarly, the NYU-VAGC (**?**),

These catalogs have been indispensible for establishing the global statistical view of galaxy properties (see **?**, for a review). previous successes with value-added catalogs

TODO what will PROVABGS be good for? extending previous statistcal analyses on SDSS to a larger sample and to higher redshift. Mention some obvious ones: stellar mass function, luminosity function, star-formation sequence. more detailed galaxy-halo connection mention some cosmological applica-

* hahn.changhoon@gmail.com
[1] https://wwwmpa.mpa-garching.mpg.de/SDSS/DR7/

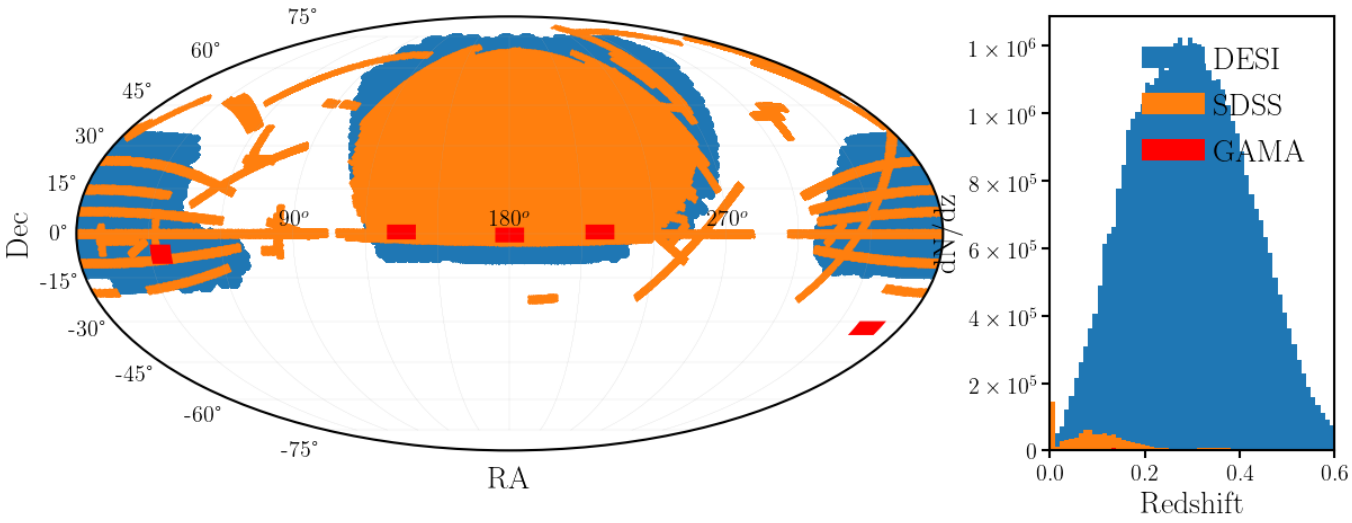

Figure 1. DESI will conduct the largest spectroscopic survey to date covering $\sim$14,000 deg^2. During dark time, DESI will measure >20 million spectra of luminous red galaxies, emission line galaxies, and quasars out to $z > 3$. During bright time, DESI will measure the spectra of $\sim$10 million galaxies out to $z\sim$0.4 with the Bright Galaxy Survey (BGS). *Left*: With its $\sim$14,000 deg^2 footprint (black), DESI will cover $\sim$2$\times$ the SDSS footprint (blue; $\sim$7000 deg^2) and $\sim$45$\times$ the GAMA footprint (orange; $\sim$300 deg^2). *Right*: Over this footprint, the BGS will provide spectra for a magnitude limited sample of $\sim$10 million galaxies down to $r < 20$, two orders of magnitude deeper than the SDSS main galaxy sample and 0.2 mag deeper than GAMA.

tions: multi-tracer analyses. Furthermore, since BGS will measure galaxy spectra down to $r \sim 20$, we will have faint dwarf galaxies at low redshift. provabgs introduces a new frontier of low signal-to-noise statistically powerful sample that will require

Why do we need a mock challenge? We want to test and cement our methodology specifically for our GQP analysis before SV data comes out. As part of the survey preparation, we have all the tools to accurately forward model observations. details on some of the specific tools and what we're able to simulate: realistic spectroscopy. realistic photometry. realistic spectro-photometry All of this gives us a rare opportunity to test our methodology on bespoke simulations.

A mock challenge is also great for testing new methodology. BGS is a bright time survey and will push the boundaries of low SNR spectra. But if we can find a way to infer robust galaxy properties the statistical payout is awesome. Something also about LRGs We're also trying to robustly fit spectra and photometry simultaneously. This has been done before (citations) but not extensively tested on simulations.

TODO

TODO

TODO

TODO

2. SIMULATIONS

DESI, with its robotically-actuated and fibre-fed spectrographs, will collect 5000 spectra simultaneously. The spectra cover the wavelength range 3600 to 9800 , with a spectral resolution of $R = \lambda/\Delta\lambda$ between 2000 and 5500. During its five-year operation, starting in 2020, it will measure over 30 million spectra over 14,000 deg^2 of the sky (cite). In addition, these DESI targets also have optical and infrared imaging data from the DESI Legacy Imaging Surveys (hereafter Legacy Surveys Dey

TODO

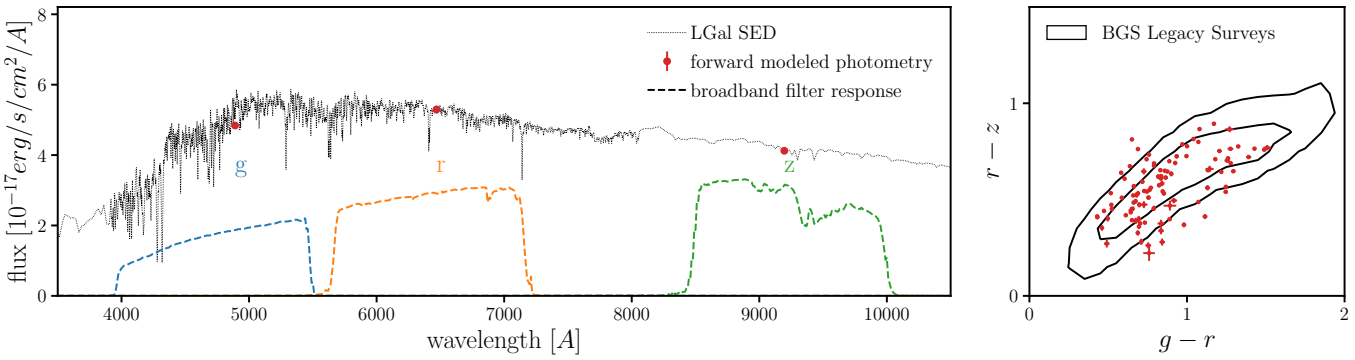

Figure 2. *Left*: We forward model DESI g, r, and z photometry (red) for our simulated galaxies (Section 2.1) by convolving their SEDs (dotted) with thei broadband filters (dashed) and then applying an empirical noise model based on BGS objects in LS (Section 2.3). *Right*: The $g-r$ and $r-z$ color distribution of the forward modeled LGAL photometry is in good agreement with the color distribution of LS BGS objects (black contours).

et al. 2019). The Legacy Surveys are a combination of three public projects (Dark Energy Camera Legacy Survey, Beijing-Arizona Sky Survey, and Mayall z-band Legacy Survey) that jointly imaged the $\sim$14,000 deg^2 DESI footprint in three optical bands (g, r, and z). Furthermore, DR8 of the Legacy Survey also includes photometry in the WISE $W1$, $W2$, $W3$, and $W4$ infrared bands. The infrared photometry is from all imaging through year 4 of NEOWISE-Reactivation force-photometered in the unWISE maps at the locations of Legacy Surveys optical sources (cite). Below we describe how we simulate realistic DESI-like galaxy spectra and photometry from state-of-the-art simulations. TODO

2.1. *L-Galaxies*

brief overview of L-GALAXIES (hereafter LGAL; Henriques et al. 2015)

2.2. *Spectral Energy Distributions*

For each simulated galaxy, LGAL provides the star formation histories (SFHs) and chemical enrichment histories (ZH) for its bulge and disk components separately, in approximately log-spaced lookback time bins. We treat each lookback time bin, i, as a single stellar population (SSP) of age t_i. Then, we derive the luminosities of the bulge and disk components by summing up the luminosities of all of their SSPs:

$$L^{\text{comp.}}(\lambda) = \sum_i \text{SFH}_i^{\text{comp.}} \Delta t_i L_{\text{SSP}}(\lambda; t_i, Z_i^{\text{comp.}}). \quad (1)$$

$\text{SFH}_i^{\text{comp.}}$ and $Z_i^{\text{comp.}}$ are the star formation rate and metallicity of the bulge or disk component in lookback time bin i. Δt_i is the width of the bin. L_{SSP} corresponds to the luminosity of the SSP, which we calculate using the Flexible Stellar Population Synthesis (FSPS Conroy et al. 2009; Conroy & Gunn 2010) model. For FSPS, we use the MIST ischrones (Paxton et al. 2011, 2013, 2015; Choi et al. 2016; Dotter 2016), the MILES spectral library (**?**), and the Chabrier (2003) initial mass function.

Next, we apply velocity dispersions to $L^{\text{comp.}}(\lambda)$. For the disk, we apply a fixed $50 km/s$ velocity dispersion; for the bulge, we derive its velocity dispersion using the Zahid et al. (2016) empirical

relation that depends on the total bulge mass. Then, we apply dust attenuation to stellar emission in the disk component ($L^{\rm disk}$) based on the cold gas content and orientation of the disk. We derive the attenuation curve using a mixed-screen model with the Mathis (1983) dust extinction curve. Stellar emission from stars younger than 30Myr are further attenuated with a uniform dust screen and a wavelength dependent optical depth. @rita further details and citations for the mixed-screen model TODO No dust attenuation is applied to the bulge component. @rita how come? TODO

Finally, we combine the attenuated disk component and the bulge component to construct the total luminosity of the simulated galaxy and then convert this luminosity to SED flux using its redshift, z.

$$f_{\rm SED}(\lambda) = \frac{A(\lambda)L^{\rm disk}(\lambda) + L^{\rm bulge}(\lambda)}{4\pi d_L(z)^2(1+z)}. \tag{2}$$

$A(\lambda)$ is the dust attenuation for the disk component described above and $d_L(z)$ is the luminosity distance. In the left panel of Figure 2, we present an example of the SED flux constructed for an arbitrary LGALgalaxy (black).

2.3. *Forward Modeling DESI Photometry*

In this section, we describe how we construct realistic LS-like photometry from the SEDs of simulated galaxies described in the last section. First, we convolve the SEDs with the broadband filters of the Legacy Survey to generate broadband photometric fluxes:

$$f_X = \int f_{\rm SED}(\lambda) R_X(\lambda) {\rm d}\lambda \tag{3}$$

where $f_{\rm SED}$ is the galaxy SED (Eq. 2) and R_X is the transmission for filter X. We generate photometry for the g, r, and z optical bands. Next, we apply realistic measurement uncertainties to the derived photometry using a simple empirical . We match each simulated galaxy to a BGS object from LS DR9 with the nearest r-band magnitude and $g-r$ and $r-z$ color. The photometric uncertainties (σ_X) and r-band fiber flux ($f_r^{\rm fiber}$ of the BGS object are then assigned to the simulated galaxy. We sample a Gaussian distribution with standard deviation σ_X and apply it to construct realistic LS-like photometry:

$$\hat{f}_X = f_X + n_X \quad \text{where } n_X \sim \mathcal{N}(0, \sigma_X). \tag{4}$$

Finally, we impose the target selection criteria of BGS (Ruiz-Macias et al. 2021, Hahn *et al.* in prep.). In the left panel of Figure 2, we overplot the forward modeled photometry (red) ontop of the SED flux (black) for an arbitrary LGALgalaxy. For reference, we also plot R_X for the g, r, and z bands of the Legacy Survey in blue, orange, and green respectively. On the right panel, we compare the $g-r$ versus $r-z$ color distribution for the forward modeled LGALgalaxies (red) to the color distribution of BGS objects in LS (black contour). The forward modeled photometry show good agreement with LS BGS objects in color space.

2.4. *Forward Modeling DESI Spectra*

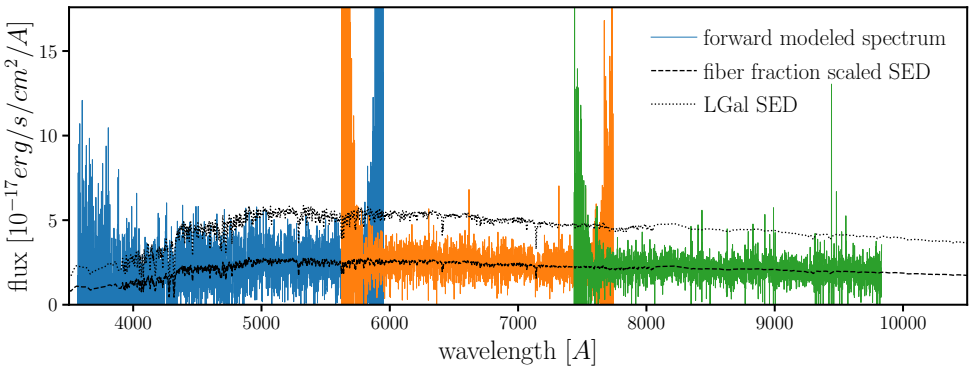

Figure 3. We construct simulated DESI spectra (solid) for LGAL simulated galaxies by applying a fiber aperture correction to the SED (dashed) and a realistic DESI noise model. We apply a fiber aperture correction by scaling down the full SED (dotted) by the r-band fiber fraction derived from the Legacy Surveys imaging. The noise model accounts for the DESI spectrograph response and an atmosphere model that accounts for the bright time observing conditions of BGS. Our forward model produces DESI-like spectra for all three arms of the DESI spectrographs: b, r, and z (blue, orange, and green, respectively). For more details, we refer readers to Section 2.4.

In this section, we describe how we construct realistic DESI-like spectroscopy from the SEDs of simulated galaxies. Our forward model involves modeling the fiber aperture effect and applying a noise model that accurately reproduces the bright time observations of BGS.

DESI uses fiber-fed spectrographs with fibers that have angular radii of 1". Only the light from a galaxy within this fiber aperture is collected by the instrument. LS provides measurements of photometric fiber flux within a 1" radius aperture ($f_X^{\rm fiber}$), which estimates the flux that passed through to the fibers. When we assign photometric uncertainties to our simulated galaxies based on r, $g-r$, and $r-z$ in Section 2.3, we also assign r-band fiber flux. We model the SED flux that passes through the fiber by scaling the SED flux by the r band fiber fraction, the ratio of the r-band fiber flux over the total r band flux:

$$f^{\rm spec}(\lambda) = \left(\frac{f_r^{\rm fiber}}{f_r}\right) f_{\rm SED}(\lambda). \tag{5}$$

This fiber aperture correction assumes that there is no significant color dependence. We also assume that there are no significant biases in the fiber flux measurements in LS due to miscentering of objects. Do we want to say more about this assumption? Also cite Marta's paper investigating aperture effect. TODO
In addition to using it for the aperture correction, we also use $f_r^{\rm fiber}$ to derive "measured" $\hat{f}_r^{\rm fiber}$:

$$\hat{f}_r^{\rm fiber} = f_r^{\rm fiber} + n_r^{\rm fiber} \quad \text{where } n_r^{\rm fiber} \sim \mathcal{N}\left(0, \frac{f_r^{\rm fiber}}{f_r}\sigma_r\right). \tag{6}$$

We later use $\hat{f}_r^{\rm fiber}$ to set the prior on the nuisance parameter of our SED modeling (Section 3).

Next, we apply a noise model that simulates the DESI instrument response and bright time observing conditions of BGS. We use the spectral simulation pipeline of cite survey simulations TODO

paper and list details [2]. More specifically, we use nominal dark time observing conditions with 180s exposure time. These conditions accurately reproduce the spectral noise and redshift success rates of observed BGS exposures in DESI survey validation data (Hahn *et al.* in prep.). In Figure 2.3, we present the forward modeled BGS spectrum of a LGAL galaxy (solid). For reference, we include the full SED (dotted) and fiber fraction scaled SED (dashed) of the galaxy.

3. JOINT SED MODELING OF PHOTOMETRY AND SPECTRA

PROVABGS will provide inferred galaxy properties derived from joint SED modeling of DESI photometry and spectra. For the SED modeling, we use a state-of-the-art stellar population synthesis (SPS) model that uses a non-parametric SFH with a star-burst, a non-parametric ZH that varies with time, and a flexible dust attenuation prescription.

The form of the SFH is one of the most important factors in the accuracy of an SPS model. In general, the form of the SFH requires balancing between being flexible enough to describe the wide range of SFHs in observations while not being too flexible that it can describe any SFH at the expense of constraining power. If the model SFH is not flexible enough to describe actual SFHs of galaxies, then unbiased galaxy properties cannot be inferred using the SPS model. For instance, most SPS models (*e.g.* CIGALE, Serra et al. 2011; BAGPIPES, Carnall et al. 2017) use parametric SFH such as the exponentially declining τ-model. Such functional forms, however, produce biased estimates of galaxy properties (*e.g.* M_* and SFR) when used to fit mock observations of simulated galaxies (Simha et al. 2014; **?**; Carnall et al. 2018). On the other hand, many non-parametric forms of the SFH are overly flexible and allow unphysical SFHs (Leja et al. 2019), which unncessarily increases parameter degeneracies and discards constraining power.

In our SPS model, we use a non-parametric SFH with two components: one based on non-negative matrix factorization (NMF) basis functions and a starburst component. For the first component, SFH is a linear combination of NMF SFH bases:

$$\mathrm{SFH}^{\mathrm{NMF}}(t, t_{\mathrm{age}}) = \sum_{i=1}^{4} \beta_i \frac{s_i^{\mathrm{SFH}}(t)}{\int_0^{t_{\mathrm{age}}} s_i^{\mathrm{SFH}}(t)\,\mathrm{d}t}. \quad (7)$$

$\{s_i^{\mathrm{SFH}}\}$ are the NMF basis functions and $\{\beta_i\}$ are the coefficients. The integral in the denominator normalizes the NMF basis functions to unity. We constrain $\sum_i \beta_i = 1$, so the total SFH of the component over the age of the galaxy (t_{age}) is normalized to unity. $\{s_i^{\mathrm{SFH}}\}$ are from Tojeiro *et al.* (in prep.) and derived from the IllustrisTNG cosmological hydrodynamic simulation (Nelson et al. 2018; Pillepich et al. 2018; Springel et al. 2018). The SFHs of simulated galaxies IllustrisTNG are compiled, rebinnined, and smoothed more details here. Afterwards, we perform non-negative matrix factorization (Lee & Seung 1999; Cichocki & Phan 2009; Févotte & Idier 2011) on the smooth SFHs to derive $\{s_i^{\mathrm{SFH}}\}$. We find that 4 components is sufficient to accurately reconstruct the SFHs from IllustrisTNG. Assuming that the SFHs of IllustrisTNG galaxies resemble the SFHs of actual observed galaxies, our NMF form provides a compact and flexible representation of the SFHs. TODO

[2] https://specsim.readthedocs.io

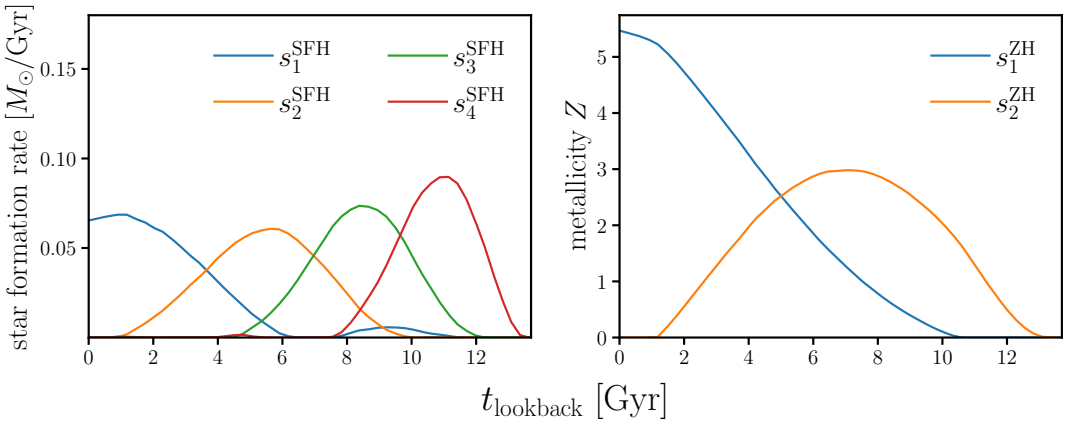

Figure 4. Non-negative matrix factorization basis functions for the SFH (left) and ZH (right). These basis functions are derived from the SFHs and ZHs of simulated galaxies in the IllustrisTNG cosmological hydrodynamic simulations.

The NMF basis functions are derived from smooth SFHs, which means that it does not include any stochasticity. However, observations and high resolution zoom-in hydrodyanmical simulations both find significant stochasticity in galaxy SFHs (**????**). To include this stochasticity in our SPS model, we include a starburst component that consists of a SSP in the SFH. For the total SFH, we use

$$\mathrm{SFH}(t, t_{\mathrm{age}}) = (1 - f_{\mathrm{burst}})\ \mathrm{SFH}^{\mathrm{NMF}}(t, t_{\mathrm{age}}) + f_{\mathrm{burst}}\ \delta_{\mathrm{D}}(t - t_{\mathrm{burst}}). \tag{8}$$

f_{burst} is the fraction of total stellar mass formed during the starburst; t_{burst} is the time at which the starburst occurs; δ_{D} is the Dirac delta function. In totatl we have 6 free parameters in our SFH: 4 NMF basis coefficients (β_i), f_{burst}, and t_{burst}.

Another key part of an SPS model is the ZH, or chemical enrichment history. Current SPS models mostly assume a ZH that does not vary over time (Carnall et al. 2017; Leja et al. 2019). Since galaxies in hydrodynamical simulations and observations do not have constant metallicities throughout their history, this assumption can significantly bias the inferred galaxy properties. Instead, for our ZH, we take a similar approach to the SFH and use NMF basis functions:

$$\mathrm{ZH}(t) = \sum_{i=1}^{2} \gamma_i s_i^{\mathrm{ZH}}(t). \tag{9}$$

$\{s_i^{\mathrm{ZH}}(t)\}$ are the ZH NMF basis functions and $\{\gamma_i\}$ are the coefficients. $\{s_i^{\mathrm{ZH}}(t)\}$ are fit using the ZHs of simulated galaxies from IllustrisTNG. We use two NMF components, so our ZH prescription has 2 free parameters.

Calzetti dust attenuation curve

Rather than evaluating the SPS directly using FSPS we use SPECULATOR, an emulator for FSPS. Brief explanation of the PCA neural net. motivate why we're using speculator by reiterating Alsing et al. (2019)s speed profiling.

describe our MCMC sampling. James's work in convergence here. talk about how in principle speculator can easily be used with HMC because you can get derivatives with backpropagation. provide detailed profiling of SED fitting and projections for full 10million galaxy BGS sample.

$$\mathrm{SFR}_{100\mathrm{Myr}} = \frac{\int_{t_{\mathrm{age}}-100\mathrm{Myr}}^{t_{\mathrm{age}}} \mathrm{SFH}(t)\,\mathrm{d}t}{100\,\mathrm{Myr}} \tag{10}$$

In Figure 3 we present the posterior as well as the best-fit photometry and spectroscopy using speculator + emcee.

4. RESULTS

Figuree 6

In order to quantify the precision and accuracy of the inferred physical properties for our simulated galaxy population, we begin by assuming that the discrepancy between the inferred and true parameters for each galaxy $\Delta_{\theta,i}$)

$$\theta_i^{\mathrm{inf}} = \theta_i^{\mathrm{true}} + \Delta_{\theta,i} \tag{11}$$

where $\Delta_{\theta,i}$ is sampled from a Gaussian distribution

$$\Delta_{\theta,i} \sim \mathcal{N}(\mu_{\Delta_\theta}, \sigma_{\Delta_\theta}). \tag{12}$$

This Gaussian distribution is described by population hyperparameters μ_{Δ_θ} and σ_{Δ_θ}, the mean and standard deviation, which quantify the accuracy and precision of the inferred physical properties for the population.

Given the photomety and spectrum of our galaxies, $\{\boldsymbol{D}_i\}$, we can get the posteriors for these population hyperparameters $\eta_\Delta = \{\mu_{\Delta_\theta}, \sigma_{\Delta_\theta}\}$ using a hierarchical Bayesian framework (**?**):

$$p(\eta_\Delta \,|\, \{\boldsymbol{D}_i\}) = \frac{p(\eta_\Delta)\; p(\{\boldsymbol{D}_i\} \,|\, \theta_\Delta)}{p(\{\boldsymbol{D}_i\})} \tag{13}$$

$$= \frac{p(\eta_\Delta)}{p(\{\boldsymbol{D}_i\})} \int p(\{\boldsymbol{D}_i\} \,|\, \{\theta_i\})\; p(\{\theta_i\} \,|\, \eta_\Delta)\; \mathrm{d}\{\theta_i\}. \tag{14}$$

Naively the posteriors for each of the galaxies are not correlated, so we can factorize the expression above

$$p(\eta_\Delta \,|\, \{\boldsymbol{D}_i\}) = \frac{p(\eta_\Delta)}{p(\{\boldsymbol{D}_i\})} \prod_{i=1}^{N} \int p(\boldsymbol{D}_i \,|\, \theta_i)\; p(\theta_i \,|\, \theta_\Delta)\; \mathrm{d}\theta_i \tag{15}$$

$$= \frac{p(\eta_\Delta)}{p(\{\boldsymbol{D}_i\})} \prod_{i=1}^{N} \int \frac{p(\theta_i \,|\, \boldsymbol{D}_i)\; p(\boldsymbol{D}_i)}{p(\theta_i)}\; p(\theta_i \,|\, \eta_\Delta)\; \mathrm{d}\theta_i \tag{16}$$

$$= p(\eta_\Delta) \prod_{i=1}^{N} \int \frac{p(\theta_i \,|\, \boldsymbol{D}_i)\; p(\theta_i \,|\, \eta_\Delta)}{p(\theta_i)}\; \mathrm{d}\theta_i. \tag{17}$$

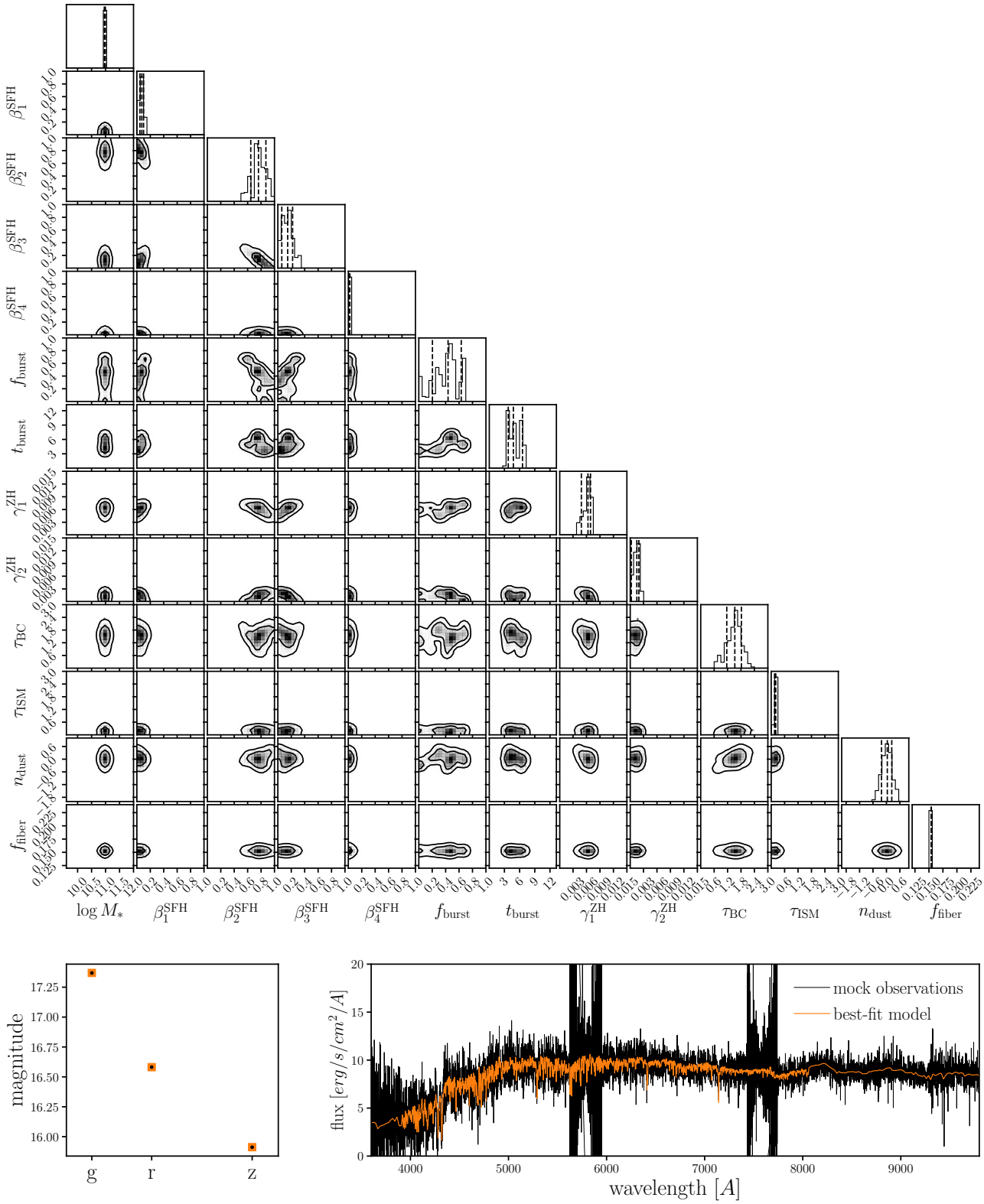

Figure 5. *Top*: Posterior probability distribution of our 12 SPS model parameters derived from joint SED modeling of the mock DESI photometry and spectra. The contours mark the 68 and 95% percentiles of the distribution. *Bottom*: Comparison of our SPS model evaluated at the best-fit parameters (orange) with the mock observations (black). On the left panel, we compare the g, r, z band magnitudes; on the right, we compare the spectroscopy.

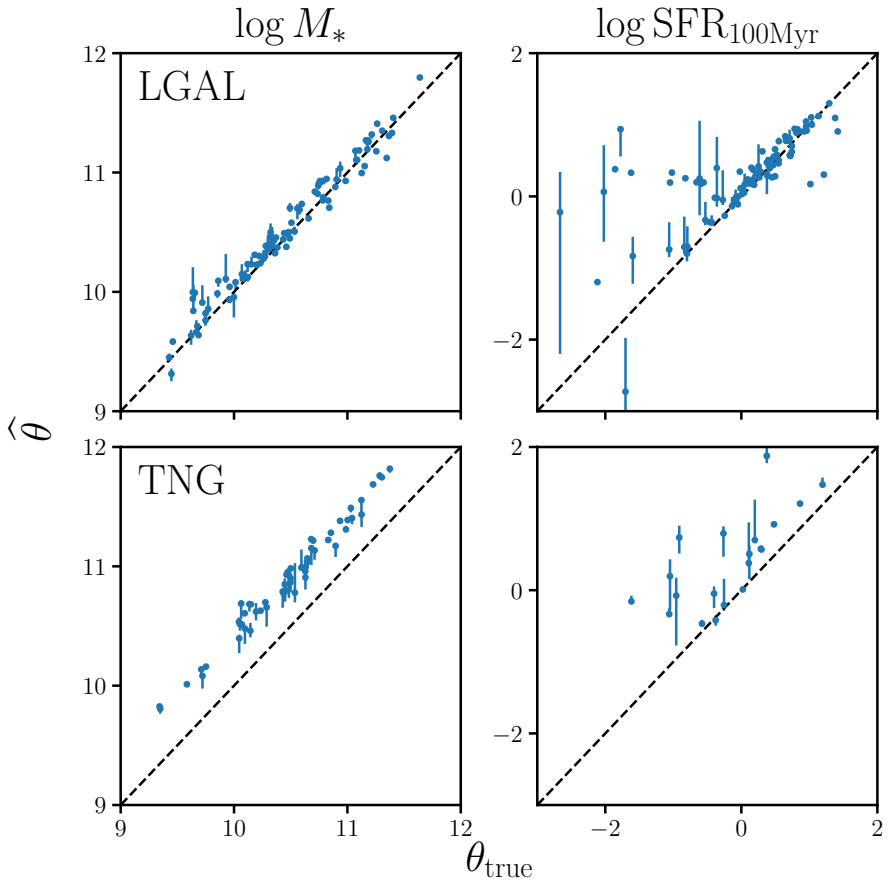

Figure 6. The properties inferred from ifsps spetrophotometry fit as a function of true properties.

$p(\theta_i \,|\, \boldsymbol{D}_i)$ is the posterior for galaxy i. Hence, the integral can be which means the integral can be estimated using the MCMC sample from the posterior

$$p(\eta_\Delta \,|\, \{\boldsymbol{D}_i\}) = p(\eta_\Delta) \prod_{i=1}^{N} \frac{1}{S_i} \sum_{j=1}^{S_i} \frac{p(\theta_{i,j} \,|\, \eta_\Delta)}{p(\theta_{i,j})}. \tag{18}$$

S_i is the number of MCMC samples and $\theta_{i,j}$ is the j^{th} sample of galaxy i. We present the maximum a posteriori (MAP) estimates of η_Δ for log M_* and log SFR in Figure 7.

η_Δ as a function of SNR/mag/colour.

discussion:

- sfh basis improves SFH accuracy?
- advantage of mcmc over MAP
- non-Gaussian posteriors
- science applicatoins
- comparison to other methods

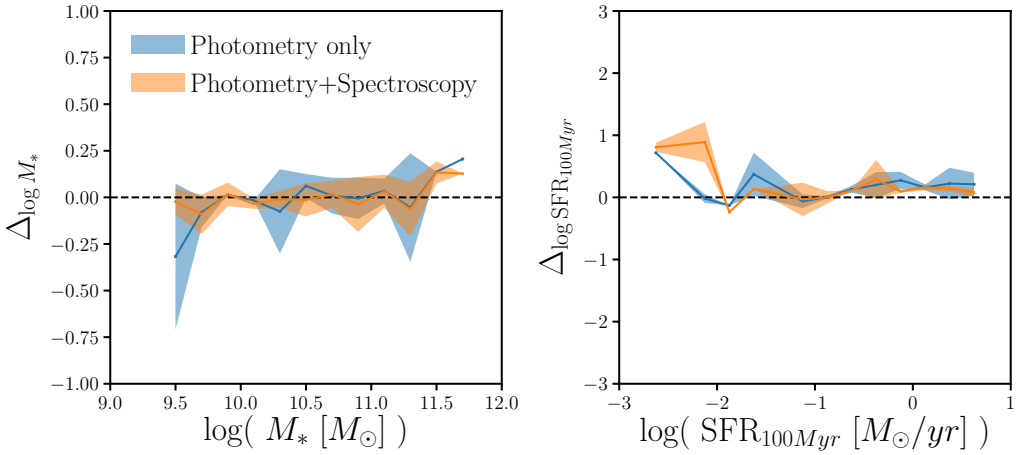

Figure 7. The discrepancies between the inferred and input/"true" M_*s (left) and SFRs (right) for our LGAL galaxies. In blue, we infer M_*s and SFRs using only photometry; in orange, we infer M_*s and SFRs by jointly fitting both photometry and spectroscopy. *Jointly fitting spectroscopy and photometry improves constraints on galaxy properties.*

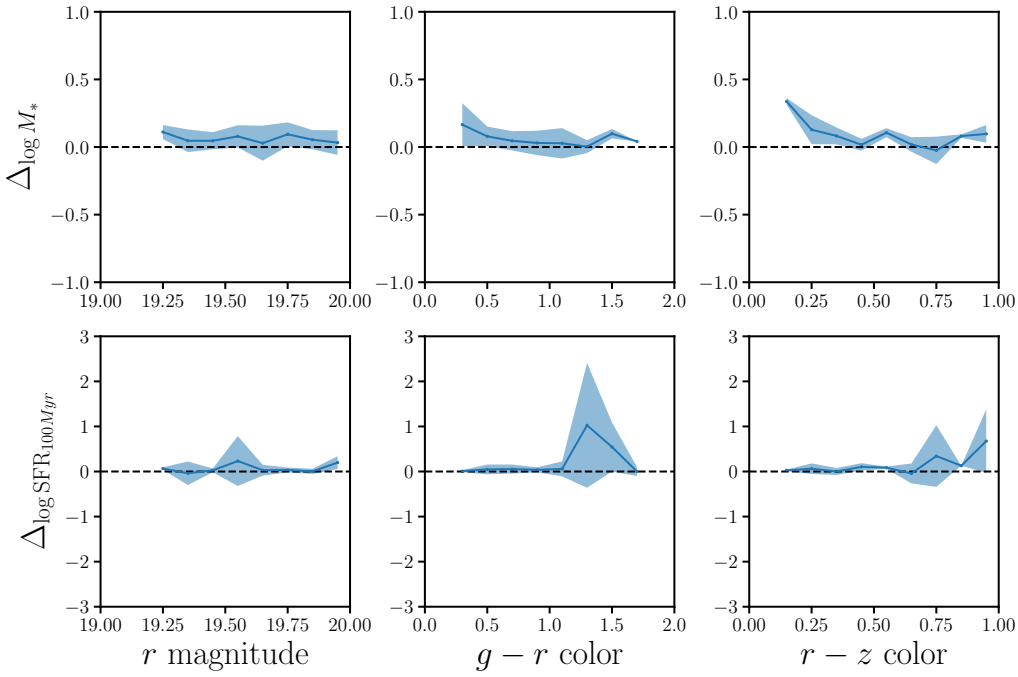

Figure 8. do we want to test bias against other properties? (e.g. obs condition?)

- different observing condition doesn't impact our results?
- we use super simple dust mmodel. **CH:** more sophistiicated dust models doesn't matter?
- **CH:** we try fitting with a different IMF

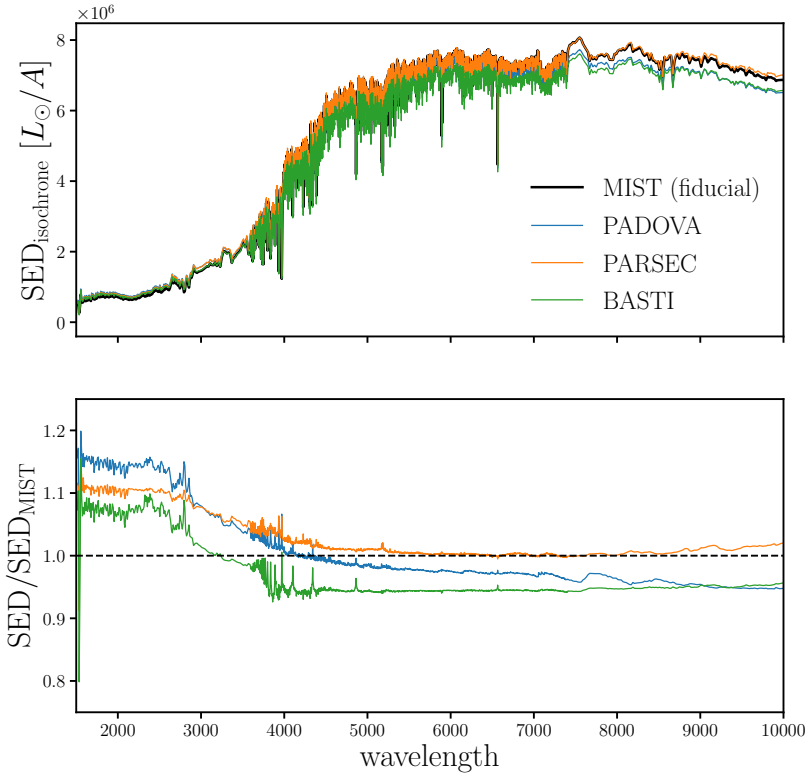

Figure 9. *Top*: Spectral energy distributions generated using MIST (black), Padova (blue), Parsec (orange), and BaSTI (green) isochrone libraries for an arbitrary set of SPS parameters. For our fiducial SED model, we use the MIST isochrone. *Bottom*: Ratios of the SEDs generated using differnt isochrone libraries over our fiducial MIST SED. The ratios reveal $> 10\%$ discrepancies at rest-frame UV wavelengths and significant offsets at higher wavelengths.

5. SUMMARY

DESI is great.

Also advertise science papers with specific focus on mock challenge science papers.

ACKNOWLEDGEMENTS

It's a pleasure to thank Joel Leja, Peter Melchior ... This material is based upon work supported by the U.S. Department of Energy, Office of Science, Office of High Energy Physics, under contract No. DE-AC02-05CH11231. This project used resources of the National Energy Research Scientific Computing Center, a DOE Office of Science User Facility supported by the Office of Science of the U.S. Department of Energy under Contract No. DE-AC02-05CH11231.

APPENDIX

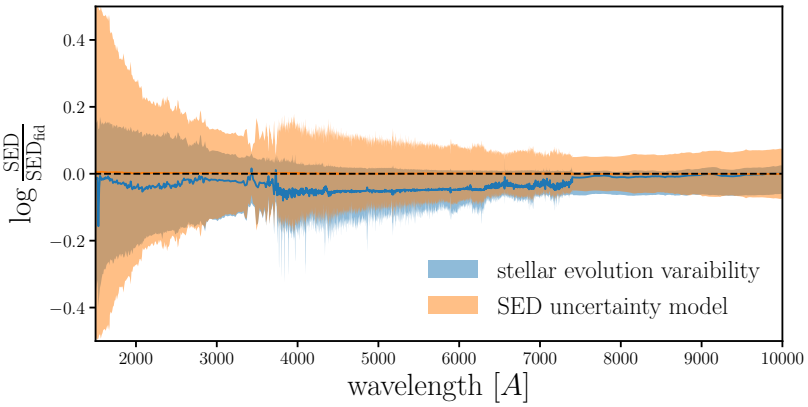

Figure 10.

Table 1. Table of $\theta_{\rm inf}$ - $\theta_{\rm true}$ and uncertainties for different CIGALE setups

set	CIGALE A	CIGALE B	CIGALE C	CIGALE D
ΔM_{tot}	0.07	0.09	0.27	0.05
M_{err}	0.13	0.20	0.16	0.16
Δ Age	1.78	1.59	1.97	1.92
Age_{err}	2.36	2.63	2.47	2.47
Δ Z	0.0037	0.0026	0.0027	0.0027
Z_{err}	0.0091	0.0085	0.0089	0.0089

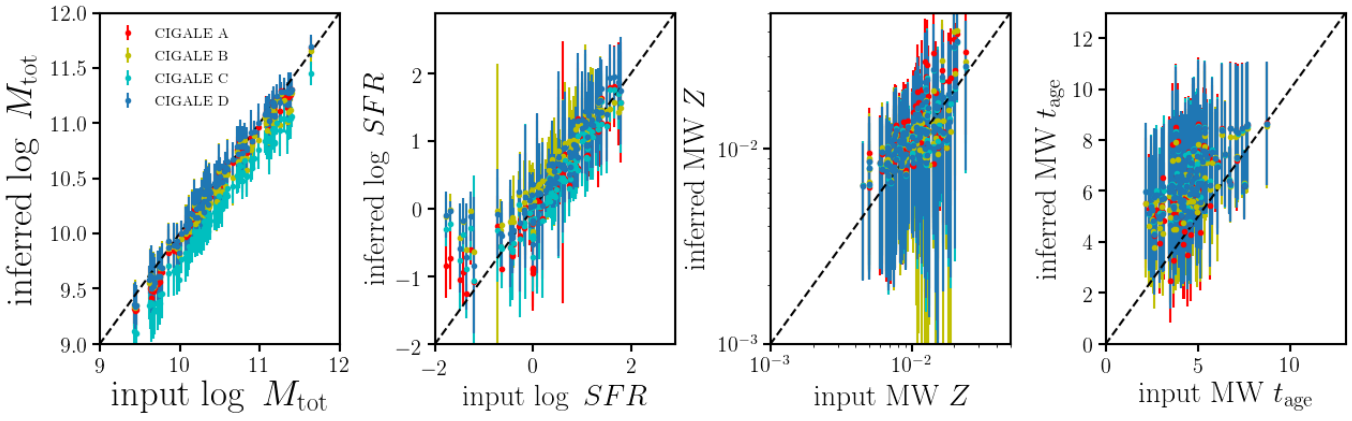

Figure 11. The properties inferred from CIGALE photometry fit as a function of true properties. Configuration CIGALE A, B, C, and D on one plot.

A. SED MODELING UNCERTAINTIES FROM STELLAR EVOLUTION

B. COMPARISON TO OTHER METHODS

REFERENCES

Alsing J., et al., 2019, arXiv:1911.11778 [astro-ph]

Carnall A. C., McLure R. J., Dunlop J. S., Davé R., 2017, arXiv:1712.04452 [astro-ph]

Carnall A. C., Leja J., Johnson B. D., McLure R. J., Dunlop J. S., Conroy C., 2018, arXiv:1811.03635 [astro-ph]

Chabrier G., 2003, Publications of the Astronomical Society of the Pacific, 115, 763

Choi J., Dotter A., Conroy C., Cantiello M., Paxton B., Johnson B. D., 2016, The Astrophysical Journal, 823, 102

Cichocki A., Phan A.-H., 2009, IEICE Transactions on Fundamentals of Electronics Communications and Computer Sciences, 92, 708

Conroy C., Gunn J. E., 2010, The Astrophysical Journal, 712, 833

Conroy C., Gunn J. E., White M., 2009, The Astrophysical Journal, 699, 486

Dey A., et al., 2019, AJ, 157, 168

Dotter A., 2016, The Astrophysical Journal Supplement Series, 222, 8

Févotte C., Idier J., 2011, arXiv:1010.1763 [cs]

Henriques B. M. B., White S. D. M., Thomas P. A., Angulo R., Guo Q., Lemson G., Springel V., Overzier R., 2015, Monthly Notices of the Royal Astronomical Society, 451, 2663

Lee D. D., Seung H. S., 1999, Nature, 401, 788

Leja J., Carnall A. C., Johnson B. D., Conroy C., Speagle J. S., 2019, ApJ, 876, 3

Mathis J. S., 1983, The Astrophysical Journal, 267, 119

Nelson D., et al., 2018, Monthly Notices of the Royal Astronomical Society, 475, 624

Paxton B., Bildsten L., Dotter A., Herwig F., Lesaffre P., Timmes F., 2011, The Astrophysical Journal Supplement Series, 192, 3

Paxton B., et al., 2013, The Astrophysical Journal Supplement Series, 208, 4

Paxton B., et al., 2015, The Astrophysical Journal Supplement Series, 220, 15

Pillepich A., et al., 2018, Monthly Notices of the Royal Astronomical Society, 473, 4077

Ruiz-Macias O., et al., 2021, Monthly Notices of the Royal Astronomical Society, 502, 4328

Serra P., Amblard A., Temi P., Burgarella D., Giovannoli E., Buat V., Noll S., Im S., 2011, The Astrophysical Journal, 740, 22

Simha V., Weinberg D. H., Conroy C., Dave R., Fardal M., Katz N., Oppenheimer B. D., 2014, arXiv e-prints, p. arXiv:1404.0402

Springel V., et al., 2018, Monthly Notices of the Royal Astronomical Society, 475, 676

Zahid H. J., Geller M. J., Fabricant D. G., Hwang H. S., 2016, The Astrophysical Journal, 832, 203